We are IntechOpen, the world's leading publisher of Open Access books Built by scientists, for scientists

6,900
Open access books available

185,000
International authors and editors

200M
Downloads

Our authors are among the

154
Countries delivered to

TOP 1%
most cited scientists

12.2%
Contributors from top 500 universities



WEB OF SCIENCE™

Selection of our books indexed in the Book Citation Index in Web of Science™ Core Collection (BKCI)

Interested in publishing with us?
Contact book.department@intechopen.com

Numbers displayed above are based on latest data collected.
For more information visit www.intechopen.com



Chapter

A Novel Drug Delivery System Based on Nanoparticles of Magnetite Fe_3O_4 Embedded in an Auto Cross-Linked Chitosan

Damiri Fouad, Yahya Bachra, Grouli Ayoub, Amine Ouaket, Ahmed Bennamara, Noureddine Knouzi and Mohammed Berrada

Abstract

Recently, chitosan (CS) was given much attention as a functional biopolymer for designing various hydrogels for industrial, environmental and biomedical applications, but their biomedical use is limited due to the toxicity of the crosslinker agents. To overcome this inconvenience, we developed an auto cross-linked material based on a chitosan backbone that carries an amino and aldehyde moieties. This new drug delivery system (DDS) was designed by using oxidized chitosan (OCS) that crosslinks chitosan (CS). In the first part, a simple, rapid, low-cost and eco-friendly green method was introduced to synthesize magnetite nanoparticles (Fe_3O_4-NPs) successfully. These nanoparticles Fe_3O_4 have received a great deal of attention in the biomedical field. Especially in a targeted drug delivery system, drug-loaded Fe_3O_4-NPs can accumulate at the tumor site by the aid of an external magnetic field and increase the effectiveness of drug release to the tumor site. In the second part, we have incorporated the Fe_3O_4-NPs into chitosan/oxidized chitosan solution because of their unique magnetic properties, outstanding magnetism, biocompatibility, lower toxicity, biodegradability, and other features. Three drugs (5-Fluorouracil (5-FU), Caffeine and Ascorbic acid)) were embedded into the magnetite solution that became quickly a hydrogel. The successful fabrication of the hydrogels and ferrogels was confirmed by (FT-IR), (TGA), (SEM), (VSM) analysis at room temperature. Finally, results showed that our hydrogels and ferrogels may be technologically used as devices for drug delivery in a controllable manner.

Keywords: magnetic nanoparticles, ferrogel, oxidized chitosan (OCS), chitosan (CS), controlled drug delivery

1. Introduction

Nowadays, the global increase in the number of people with chronic diseases as "cancer, diabetes, etc." have affected the health and quality of life of many citizens around the world. For example, cancer is considered a public health problem because of its high incidence and mortality. The World Health Organization (WHO)

estimates 27 million cases of cancer and 17 million deaths disease for the year 2030 [1]. Therefore, study on cancer treatment has attracted many scientists. Among therapies, cancer chemotherapy is widely used despite its disadvantages. Chemotherapy usually causes serious side effects because of the low selectivity of anti-cancer drugs, which affects not only cancer cells but also normal cells [2]. Thus, increasing attention is being paid to targeted drug delivery systems, which have been used to increase the efficiency of drug delivery to specific tissues and to decrease the associated side effects.

The most efficient solution is to use nanoparticles embedded in the hydrogel; this innovative-targeted drug delivery strategy involves coupling the drug to magnetic nanoparticles (NP_s) that can be guided to the target using external magnetic fields [3]. Once they reach the target, the nanoparticles release the drugs under the influence of an alternating magnetic field [4]. Nanoparticle (NP) targeting has shown great potential for cancer drug delivery applications over the past decade. From nanoparticle targeting, magneto-particle have been widely studied because of their ability to target when an external magnetic field is applied [5].

An increasing population causes serious environmental pollution, waste production is also increasing and major proportion of by-products generated by contemporary food remains underused which may often contain precious substances. The crucial problem confronting by industries and society in food processing is the elimination of food waste. Chitin is an important natural resource and the world's annual production of it is approximately 10^{10}–10^{12} tons [6]. This latter is principally produced by mollusks, arthropods (crustaceans and insects) and fungi [7]. However, chitin and its derivatives have a high economic impact due to their numerous applications in the pharmaceutical [8], food [9, 10], cosmetics [11], textile [12], wastewater treatment and agricultural sectors [13].

In the past few decades, drug delivery systems (DDS) have been of great interest and resulted in many efforts to realize the effectiveness and targeted drug delivery tendency as well as to reduce the associated side effects [14]. However, DDS provide several advantages as compared to conventional dosages in terms of improved efficacy, reduced toxicity, improved patient compliance, and convenience [15]. Thus, the carriers used for drug release are generally biodegradable polymers which are extensively used for designing the control drug delivery systems [16].

On the other hand, with the rapid development of technology much attention has been given to use biopolymer based hydrogels in many applications including pharmaceuticals [17, 18], cosmetics [19], agriculture [20] and biotechnology [21, 22]. However, porous biomaterials fabricated from natural polymers "chitosan" were given significant attention for years. Chitosan is a unique natural cationic biopolymer produced by N-deacetylation of chitin and is the second most abundant natural polymer after cellulose [23]. Chitosan has been widely used in the biomedical field due to its superior properties including good biodegradability [24], biocompatibility [24], low toxicity [25, 26], mucoadhesive properties [27], antibacterial activity [28] and low cost [24, 29]. Chitosan is an excellent candidate for different applications particularly it has been employed in various FDA (Food and Drug Administration) approved biomedical applications. The $-NH_2$ group of the (CS) chains is a pH-sensitive polymer with pK_a around 6.5 due to variation of charge density at the pH range of 6–6.5, which is useful for wide range of pharmaceuticals applications. The pH value of the soluble-insoluble transition in the range 6–6.5 [30]. At pH levels beneath the pK_a, high charge density of chitosan results in polyelectrolyte formation, in contrast at neutral pH, the low charge density of chitosan eases the intracellular release of biomolecules and contributes to its low cytotoxicity [31]. Chitosan has increasingly been used in the pharmaceutical field as it is one of the excellent choices for the Schiff's base linkages to form an injectable hydrogel due to the nature of abundant amino groups on its backbone. Hydrogels from chitosan

are usually prepared through physical interchain interaction or chemical reaction of the free amine groups with crosslinker agents (e.g. glutaraldehyde, glyoxal [32]). The disadvantage of these crosslinking agents, especially glutaraldehyde [33], benzaldehyde [34] and glyoxal is their toxicity to human tissues even at small traces [35], which has limited the use of chitosan hydrogels as scaffolds for drug delivery.

However, this paper discusses the recent trends in drug delivery systems (DDS) applications using macroscopic hydrogels. Hydrogel has received extensive attention due to its interconnected cross-linked porous hydrophilic polymer networks which can absorb large amounts of water or biological fluids. Additionally, hydrogels can be divided into three categories according to their size: macroscopic gels, nanogels (<200 nm), and microgels (0.5–10 μm). Hydrogels are promising, fashionable, intelligent and "smart" drug delivery vehicles that meet specific requirements for targeting drugs to specific sites and controlling drug release. The hydrogel-based drug carrier loaded with 5-fluorouracil (5-FU) drug for an up to 36 days sustained delivery has been studied by Xueyun Chen et al. [36].

Hydrogels are trendy, promising, intelligent and 'smart' drug delivery vehicles have become a great search field for targeting drugs to the specific sites and controlling drug release. Among several hardware platforms, ferrogels (FG) have a high potential for use in drug delivery. Ferrogels (FG) are consisting mainly of a polymer matrix embedded with magnetic micro and nano-particles (Fe_3O_4) [37–39]. Upon the application of an external magnetic field, the polymer matrix of the ferrogel can deform due to the magnetic force generated by the embedded magnetic particles, which would allow actuation and magnetically driven drug release on demand. The main advantage of ferrogels is that a larger quantity of drug can be loaded, compared to that transported by simple magnetic dispersion nanoparticles.

Ferrogel (FG) are typically prepared by incorporating magnetic particles into hydrogels [40]. Magnetic nanoparticles (Fe_3O_4) shown in **Figure 1**, have attracted much attention in the last few years as carriers for drug delivery systems. The potential use of nanoparticles as drug carriers has been presented in recent years as a major challenge, as nanoparticles have been designed to improve pharmacological and therapeutic effects in terms of reducing their toxic side effects. Besides, magnetite (Fe_3O_4) is considered as an important type of magnetic material with cubic inverse spinel structure. This property makes it very interesting because of its wide field of use, including magnetic recording, ferrofluid [41], catalyst [42] and some biomedical applications like magnetic resonance imaging (MRI) [43], bio separation [44], in addition to drug delivery system and therapeutic hyperthermia as well, to treat cancer and tumors [45]. Several methods have been developed recently

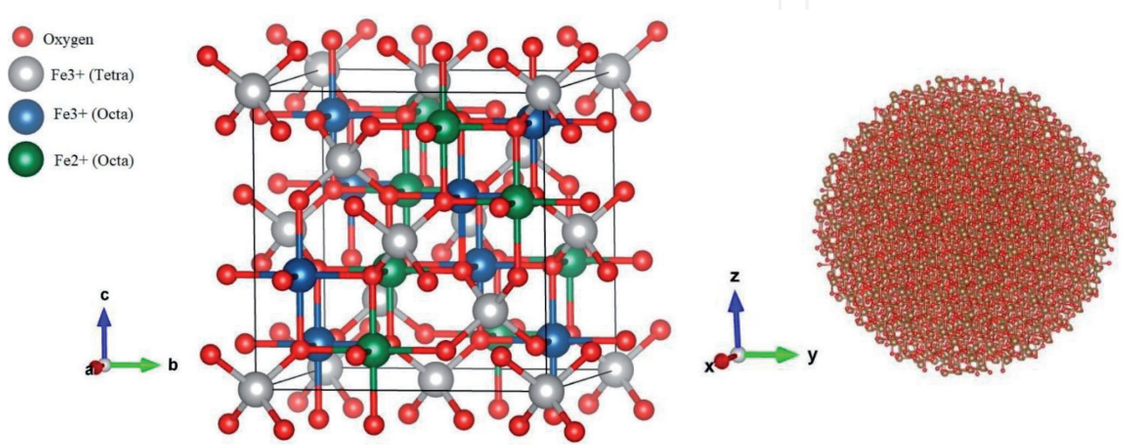


Figure 1.
Model of crystal structure of magnetite (Fe_3O_4) and spherical Fe_3O_4 nanoparticles.

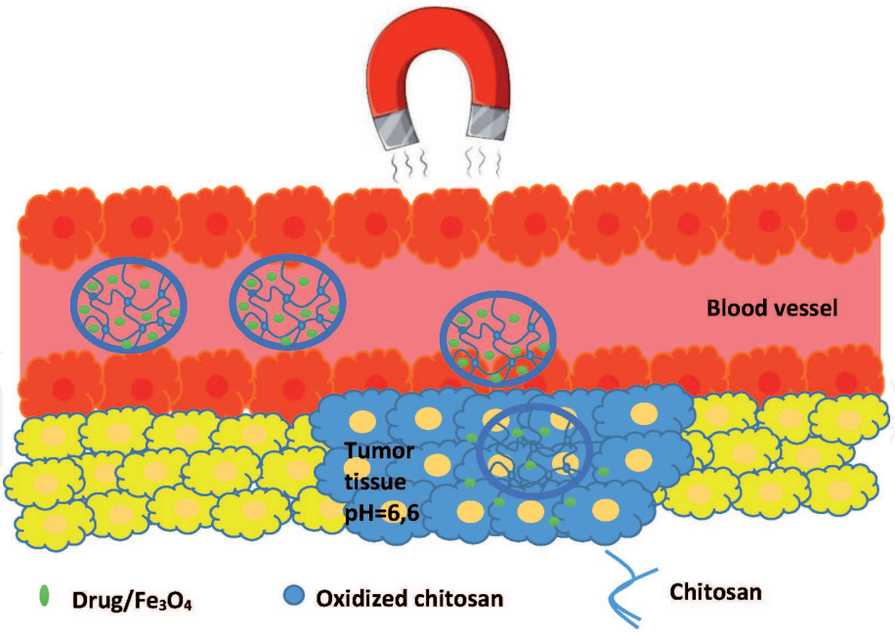


Figure 2.
Schematic representation of magnetic drug delivery system under the influence of external magnetic field.

for preparing magnetic nanoparticles, such as co-precipitation [46], sol–gel [47], solvothermal [48], sonochemical and chemical vapor deposition phase (CVD) [49]. Among these methods, co-precipitation is considered as the simplest, most efficient, and most economic method.

Ferrogels characterized by the presence of magnetic particles incorporated in polymer gels, are the subject of extensive research due to those magnetic particles and magnetic fields which have an extended application and clinical acceptance [50, 51]. Recent studies have shown controlled release of many drugs from ferrogels subject to magnetic fields [52, 53]. Ferrogels (FG) have made also injectable and biodegradable. However, typical drug delivery ferrogels have a disadvantage due to the cross-linking agent toxicity, which limits the macroporous biomaterials synthesis [37].

There are only a few reports in the literature on the synthesis of Fe_3O_4 by co-precipitation method. In this paper, a macroporous ferrogel which is sensitive to magnetic field was studied. Furthermore, we are probably the first scientific team that reports the preparation of novel hydrogels and ferrogels based on chitosan and oxidized chitosan as cross-linking agent embedded Fe_3O_4/drug (5-FU, caffeine and ascorbic acid). **Figure 2** shows the magnetic drug delivery system under the influence of external magnetic field. The kinetics and in-vitro drug release profile of the drugs were studied in PBS pH (7.4) buffered solution at 37°C.

2. Materials and methods

2.1 Materials

Chitosan (in powder form was prepared in our laboratory from exoskeletons of shrimp waste and purified, with degree of deacetylation >90% was determined by conductimetric titration), iron (II) sulfate heptahydrate ($FeSO_4.7H_2O$, sigma-Aldrich), iron (III) chloride ($FeCl_3.6H_2O$, Sigma-Aldrich), Caffeine (sigma-Aldrich), 5-Fluorouracil (sigma-Aldrich), Ascorbic acid (Fluka), Sodium metaperiodate ($NaIO_4$, sigma-Aldrich), Hydrochloric acid (sigma-Aldrich), Ethylene glycol (sigma-Aldrich), Acetic acid (sigma-Aldrich), Sodium bicarbonate (Panreac), Sodium hydroxide (Sigma-Aldrich).

2.1.1 Synthesis of oxidized chitosan (OCS)

Oxidized chitosan (**Figure 3**) was prepared according to a previously reported method [54, 55]. The purified chitosan (1 g) ([GlcN] = 5.34 mM) was dispersed in 50 ml Hydrochloric acid solution HCl (10^{-3} M) at pH ranging from 4 to 5, and kept under magnetic stirring at 4°C for 30 min. Then 1 ml aqueous solution of sodium periodate 0.534 mM, P_0 = 0.1 (P_0 = moles of $NaIO_4$ x moles of GlcN) was added to the mixture. The reaction system was covered with aluminum foil to prevent photo induced decomposition of periodate ion. The reaction lasted for 30 min at 4°C and it was interrupted by the addition of 1 ml ethylene glycol to inactivate any unreacted periodate in a molar ratio of 1:1. The oxidized derivative was washed by distilled water for 5 h and the dry product was obtained by freeze-drying.

2.1.2 Preparation of oxidized chitosan (OCS)/chitosan (CS) hydrogels

The procedure for preparation of the hydrogel was as follows: chitosan (0.1 g) was dispersed in 10 ml of (1% acetic acid) at pH = 4.8 in an ice bath under magnetic stirring until a clear solution was obtained. Afterwards, the drug (5-FU 10 mg, Caffeine 10 mg or Ascorbic acid 10 mg) was added into the solution and gently stirred until the complete dissolution for 30 min. The oxidized chitosan (60 mg) was added to the solution of chitosan soluble drug under continuous stirring to facilitate crosslinking between amino of chitosan (NH_2) and aldehyde groups of chitosan (OCS). Then the 6% (w/v) $NaHCO_3$ solution was slowly added to the solution in an ice bath under magnetic stirring to get homogeneous mixture at pH = 7 [56], and a transparent gel was obtained as shown in **Figure 4**. The hydrogel was washed with ethanol, and filtered to remove traces of unreacted reagents.

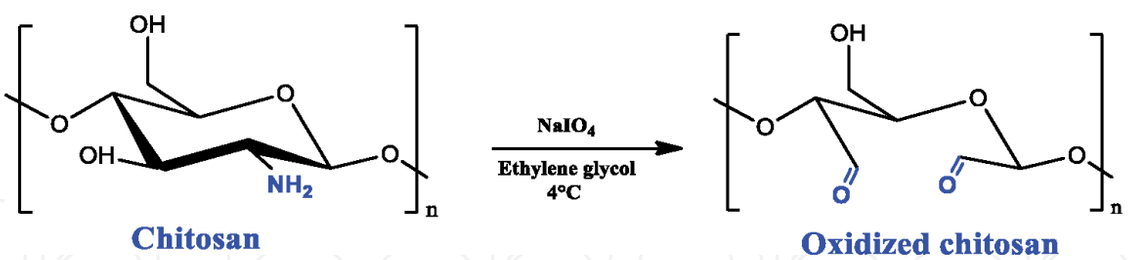


Figure 3.
Schematic representation of reaction between chitosan (CS) by sodium periodate.

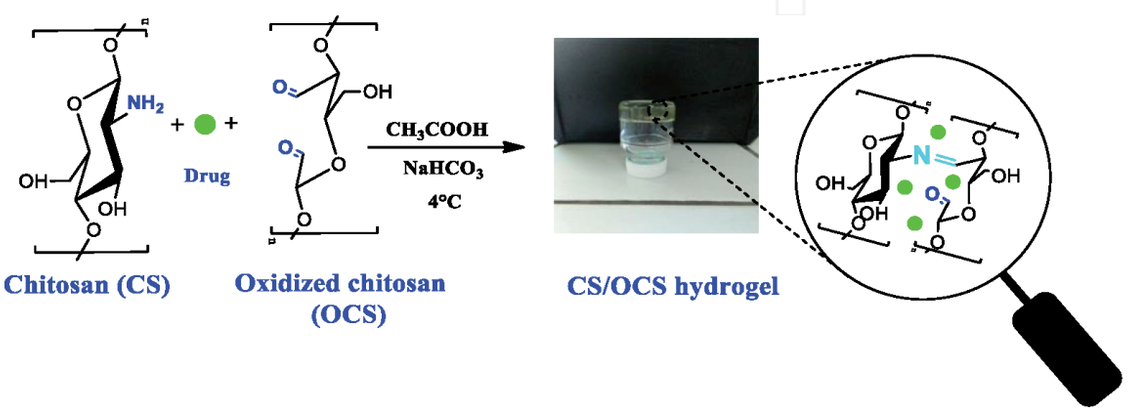


Figure 4.
Schematic representation of the chemical (CS)/(OCS) cross-linking mechanism and the formation of the hydrogel.

2.1.3 Synthesis of magnetite nanoparticles (Fe3O4) by co-precipitation

According to the previous work, magnetite (Fe_3O_4) nanoparticles were synthesized by chemical co-precipitation method. Magnetic Fe_3O_4 NPs were synthesized by dissolving 50 mL of $FeCl_3.6H_2O$ and 25 mL of $FeSO_4.7H_2O$ in 350 mL of distilled water under nitrogen atmosphere under vigorous stirring. Upon addition of (35 ml) NaOH, the pH was adjusted to about 10, the solution turned black, indicating the formation of magnetite nanoparticles. Further stirring is continued for 1 h to uniformly disperse the magnetic nanoparticles. After raising the reaction temperature to 80°C. Then, a formed black precipitate was collected with an external magnet, washed several times with ethanol and distilled water, and dried in vacuum at 60°C. The entire reaction is given by the equation as shown in **Figure 5**.

2.1.4 Synthesis of ferrogel

Firstly, chitosan solution was prepared by dissolving 0.1 g chitosan (CS) in 10 mL acetic acid solution (1%). 50 mg iron oxide nanoparticles were mixed with chitosan solution and stirred for 2 h at 40°C to give chitosan coated magnetic nanoparticles (CS-Fe_3O_4). Then, the drug (5-FU 10 mg, Caffeine 10 mg or Ascorbic acid 10 mg) was added into the solution (CS-Fe_3O_4) and gently stirred for 30 min. 60 mg of oxidized chitosan (OCS) was added as crosslinking agent and were mixed with (CS-Fe_3O_4) solution. The reaction mixture was stirred at 0°C for 3 hours. The pH of the solution was adjusted to pH = 7 with 6% (w/v) $NaHCO_3$. The product (CS-Fe_3O_4-OCS) was washed with deionized water. **Figure 6** shows a representation of the prepared drug delivery ferrogel.

2.1.5 Fourier transform infrared (FTIR) spectra of hydrogel

Fourier transform infrared (FTIR) spectra of the chitosan, oxidized chitosan, CS/OCS hydrogel, CS/drug/OCS lyophilized hydrogel, Fe_3O_4 NPs and the

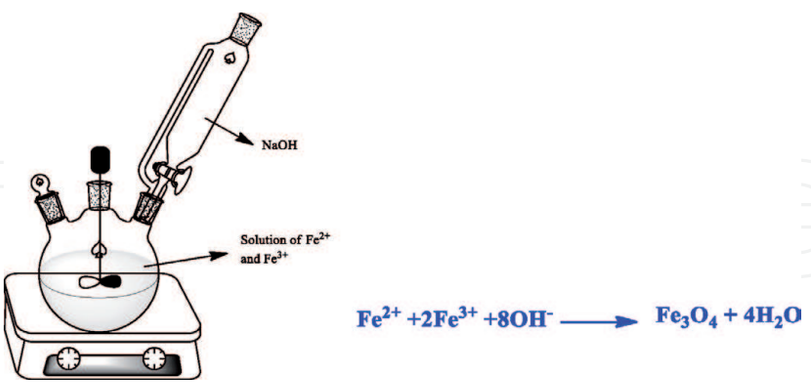


Figure 5.
Representation of superparamagnetic magnetite nanoparticles synthesis technique.

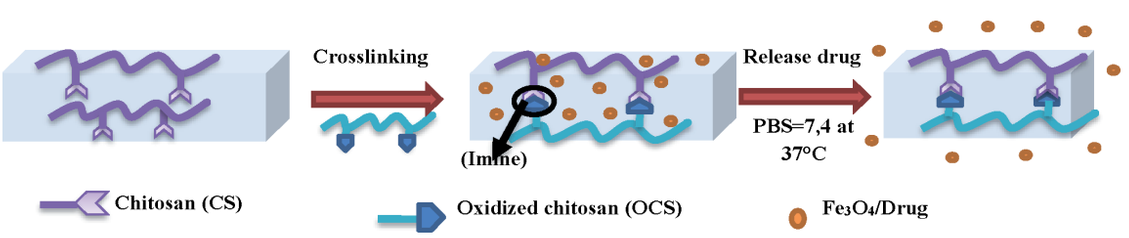


Figure 6.
Representation of superparamagnetic drug delivery hydrogel.

freeze-dried CS/Fe_3O_4/OCS ferrogel were obtained from discs containing 2.0 mg dry sample in approximately 198 mg potassium bromide (KBr). The measurements were recorded by a Perkin–Elmer FTIR spectrophotometer at the resolution of 4 cm^{-1} in the wave number region 400–4000 cm^{-1}.

2.1.6 Thermogravimetric (TGA) analysis

The thermal properties of lyophilized hydrogel, pure chitosan, oxidized chitosan, Fe_3O_4 NPs and CS/Fe_3O_4/OCS lyophilized ferrogel were investigated by thermogravimetric analysis (TGA). Samples were placed in the balance system and heated from 40 to 800°C at a heating rate of 10°C/min using a TA Instruments TGA (Q_{500}) device.

2.1.7 Magnetization studies using (SQUID) analysis

The saturation magnetization of Fe_3O_4 NPs, CS-Fe_3O_4-OCS ferrogel was measured by vibrating sample magnetometer VSM (SQUID model MPMS XL 7) from Quantum at room temperature between magnetic fields of −14,000 (Oe) to 14,000 (Oe).

2.1.8 Scanning electron microscopy (SEM)

The chitosan-based hydrogels cross-linked with oxidized chitosan was frozen at −75°C for 24 h and then lyophilized (by Alpha 1–2 LD_{plus}) for 48 h. The lyophilized sample was obtained and then examined by a scanning electron microscopy (SEM) (Mini SEM Hirox SH-4000).

2.1.9 Hydrogel swelling

Freeze-dried CS/OCS hydrogel were immersed in phosphate-buffered saline (PBS) at 37°C (pH = 1.2, pH = 5.8 and pH = 7.4). The samples were weighed before being put into PBS (W_0). After the vial was sealed and held at 37°C for 24 h, and the excess solution on the surface of the hydrogels was quickly absorbed with filter paper [55]. The equilibrium-swelling ratio (SR) was calculated using the following equation:

$$\mathbf{SR}\% = \frac{\mathbf{W_s} - \mathbf{W_d}}{\mathbf{W_d}}, \quad (1)$$

where, W_d is the weight of dry hydrogel after lyophilization and W_s is the weight of swollen hydrogel.

2.1.10 In vitro drug release from the hydrogels and ferrogels

(5-FU, caffeine or ascorbic acid) was selected and used as a model drug in the release experiments. In vitro drug release test was performed in a phosphate buffer solution PBS (pH 7.4 at 37°C) under shaking. The hydrogels and ferrogels (m = 1.14 g) (3 cm x 4 cm) were placed in a cartouche before immersing in 1000 mL of phosphate-buffered saline (PBS). At predetermined time intervals, 5 mL of release medium was withdrawn. Then 5 mL of fresh buffer was added to the original to maintain the total volume. The drug release was determined by

UV–Vis spectrophotometry at λ_{max} (5-Fluorouracil (266 nm), caffeine (273 nm) and ascorbic acid (265 nm)). The concentration of the active ingredient in the (PBS, pH = 7.4 at 37°C) has been achieved from the calibration curve, and the amount of drug released at time t (M_t) was calculated by accumulating the total active ingredient release up to that time. In vitro drug release tests were performed in triplicate (n = 3). There are a few steps, which mainly control drug release phenomena from the polymer matrix, dissolution of the drug, liquid penetration into the matrix and diffusion of the drug from the drug encapsulated in the matrix. In order to understand the release kinetics and the mechanism of the active ingredient release, release kinetics data obtained in vitro using ferrogels and hydrogels are fitted with kinetics model. The release data are best fitted with the Korsmeyer–Peppas (KP) model. The (KP) model deal with Eq [57]:

$$\%\textbf{Cumulative release} = \frac{\mathbf{M_t}}{\mathbf{M_0}} \times \mathbf{100} \tag{2}$$

where "M_t" is the amount of drug released at time (t), "M_0" is the maximal amount of the drug released at maximum interval. It is interesting to note that three drugs (5-FU, caffeine and ascorbic acid) in hydrogels exhibit a Fickian nature of drug diffusion. However, the interaction of the drug molecules with the matrix play an important role in the drug release kinetics occurring through a diffusion mechanism.

2.2 Statistical analysis

The experimental data are expressed as the mean values of at least three replicates ± standard deviation (SD). The results were analyzed and showed usage Kaleida graph.

3. Results and discussion

3.1 Hydrogel and ferrogel formation

The concept of this study is depicted in (**Figure 7**). Oxidized chitosan (OCS) was prepared following a well-known method where chitosan is oxidized with sodium periodate ($NaIO_4$). Oxidization of chitosan created multiple aldehyde groups all along the polymeric chain using the method described in literature [54, 58]. The hydrogels and ferrogels (magnetic Fe_3O_4 embedded in novel hydrogel) were prepared by crosslinking chitosan (CS) with oxidized chitosan (OCS). The crosslinking of hydrogel and ferrogel was achieved by (–C=N-) bonds of Schiff-base reaction. Our results indicate that the process synthesis of the hydrogel and ferrogel was embedded with three drugs (5-FU, caffeine and ascorbic acid) has successfully loaded in the carrier polymeric. The schematic representation of smart ferrogel "magnetic hydrogel" was shown in (**Figure 7**).

The **Figure 8** shows the procedure for preparation of the hydrogel and a photograph of (CS-drug-OCS) hydrogel.

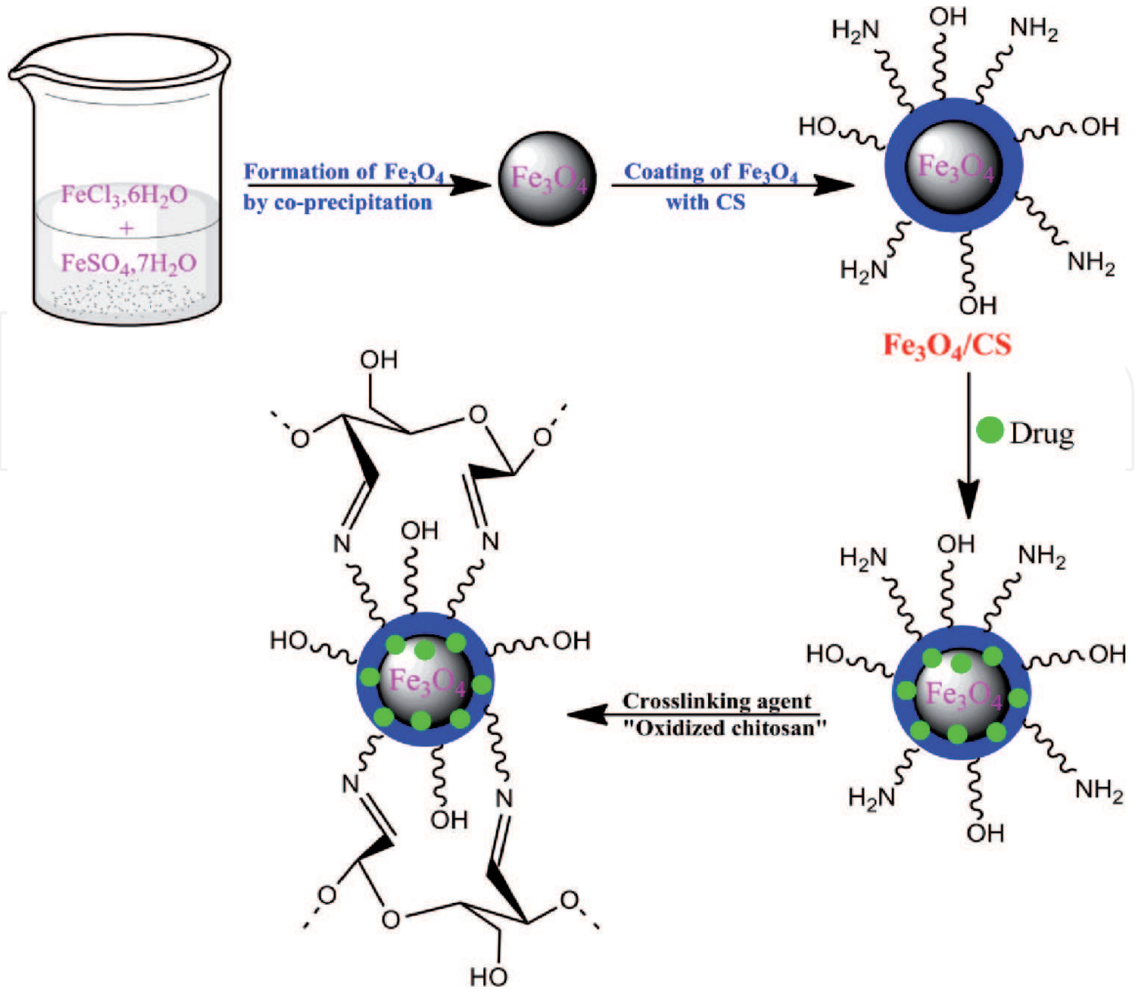


Figure 7.
Schematic representation of (CS-Fe_3O_4-OCS) ferrogel.

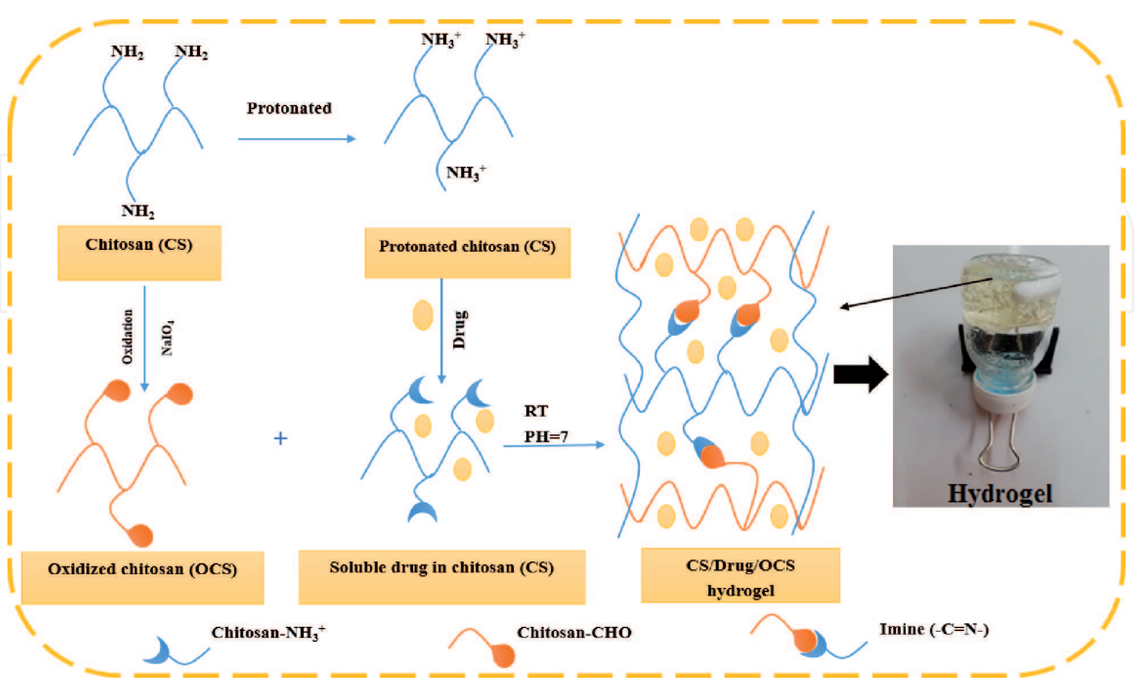


Figure 8.
Schematic representation of the synthesis process of CS/drug/OCS hydrogel.

3.2 Fourier transform infrared (FTIR) spectra of hydrogel

The IR spectrum of CS, OCS, (CS/OCS) and (CS/drug/OCS) lyophilized hydrogel are listed in (**Figures 9** and **10**) and major functional moieties are labeled with wavenumbers was recorded in the region of 4000–40 cm^{-1}. The FTIR spectrum of pure chitosan (**Figure 9(a)**) shows wide band around 3450 cm^{-1} corresponding to amine N–H symmetrical vibration and H bonded O–H group. The peak observed between 3400 and 3700 cm^{-1} corresponding to combination of the band O-H, NH_2 intra and intermolecular hydrogen bonding. The peaks at 2920 and 2320 cm^{-1} are assigned to the symmetric and asymmetric may be attributed to –CH vibrations of carbohydrate ring [59]. The bands at 1650 cm^{-1} and 1545 cm^{-1} may be attributed to C=O stretching (amide I vibration) and N-H bending (–NH_2 bending of amide II) in amide group, respectively and 1390 cm^{-1} (N–H stretching or C–N bond stretching vibrations, amide III vibration) [60]. The peak observed at 1050 cm^{-1} has the contribution to the symmetric stretching of C–O–C groups. The absorption peaks in the range 900–1200 cm^{-1} are due to the antisymmetric C–O stretching of saccharide structure of chitosan. In order to understand the oxidation of oxidized chitosan (OCS), the FTIR spectra results for (OCS) in (**Figure 9(b)**) verified successful oxidation, while a new absorption peak appeared around 1725 cm^{-1} [55], which was assigned to an aldehyde group (-C=O) bond, indicating that the CS has been successfully oxidized by the $NaIO_4$ [61]. Furthermore, the peak (**Figure 9(c)** at 1637 cm^{-1} caused by C=O and C=N is reduced significantly. These differences indicate that the aldehyde groups of OCS reacted with the amino groups of CS to generate a Schiff base"imine" [62]. FTIR analysis was performed (**Figure 9(d)**) exhibits the IR spectra of the prepared nanoparticles. The spectrum of Fe_3O_4 magnetic nanoparticles shows the formation of two strong absorption bands between 636 cm^{-1} and 592 cm^{-1}. Furthermore, the band at 592 cm^{-1} was confirmed as the Fe-O stretching vibration of tetrahedral sites of spinel structure. The absorption bands at 459 cm^{-1}, assigned to tetrahedral and octahedral sites, peaks at 3400 cm^{-1} due to the O-H stretching model adsorbed on the surface of the Fe_3O_4 nanoparticles [63].

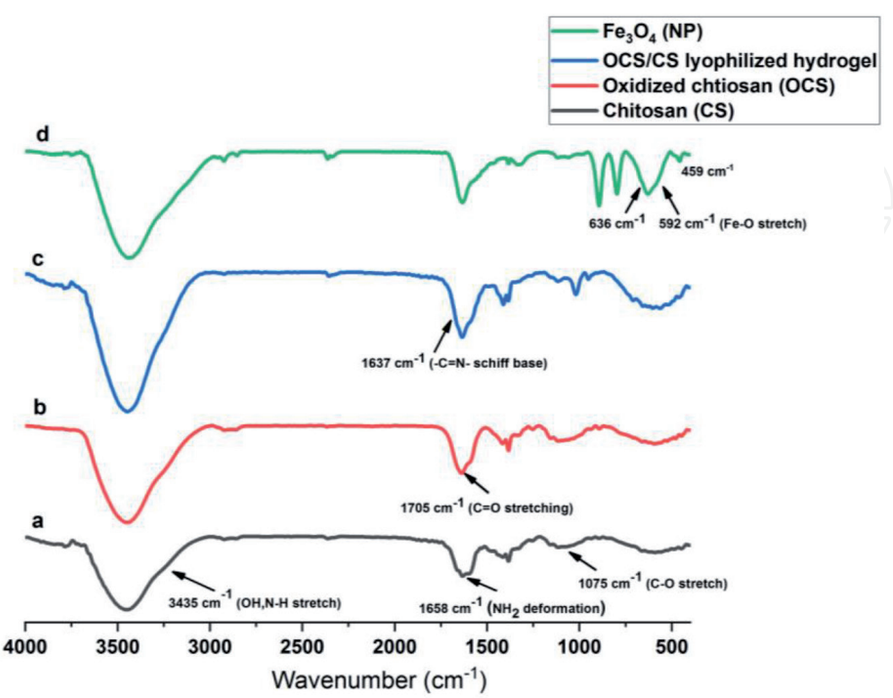


Figure 9.
FTIR spectra of (a) chitosan, (b) oxidized chitosan, (c) CS/OCS lyophilized hydrogel, (d) Fe_3O_4 NP.

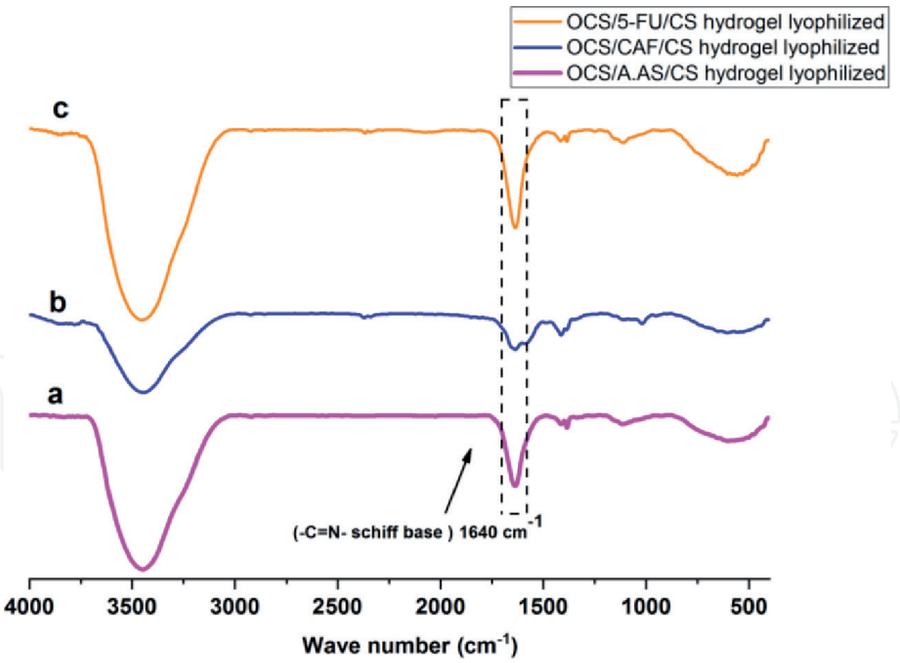


Figure 10.
FTIR spectra of (a) CS/a.AS/OCS lyophilized hydrogel, (b) CS/CAF/OCS lyophilized hydrogel; (c) CS/5FU/OCS lyophilized hydrogel.

For the spectra of three drugs (5-FU, caffeine and ascorbic acid) loaded (CS/OCS) in hydrogels (**Figure 10**); exhibited the characteristic absorption of imine stretching vibration (-C=N–) at 1637 cm^{-1} [54, 64], suggests that the coupling reaction was occurred between –CHO of OCS and $–NH_2$ of CS.

3.3 Magnetization studies using (SQUID) analysis

The measurements of the magnetic field-dependence of the magnetization of the uncoated and coated magnetite nanoparticles at 25°C are presented in (**Figure 11**). The plots indicate that both samples exhibit superparamagnetic behavior with zero remanence and coercivity. (**Figure 11**) shows the magnetic curves as a function of applied field at room temperature obtained for Fe_3O_4 and CS-Fe_3O_4-OCS ferrogel, respectively. The magnetization saturations were found to be 60.57 emu/g for Fe_3O_4, 17.25 emu/g for CS-Fe_3O_4-OCS ferrogel [65]. The magnetization value decreased after coating due to the existence of oxidized chitosan and chitosan, which formed polymerized multilayers. It can be concluded that the Ms. value of CS/Fe_3O_4/OCS ferrogel is less than the Fe_3O_4 (NPs) that can be attributed to the creation of a non-magnetic polymer layer around Fe_3O_4 (NPs) in the hydrogel [66]. Taking into account the magnetic properties of the prepared by ferrogel, it may be able to deliver the drug to the target area in the presence of an external magnetic field.

3.4 Scanning electron microscopy (SEM)

A perfect injectable hydrogel must have pores in the range of 50–100 μm and a high degree of interconnectivity to facilitate nutrient and oxygen transport, as well as cell adhesion and migration. By using SEM, we studied the pore size distribution in hydrogels (**Figure 12**). In this study, morphology of freeze-dried hydrogel (CS/OCS) were observed with scanning electron microscope (SEM). As can be seen in (**Figure 12**), the (CS/OCS) lyophilized hydrogel had continuous and porous structures with interconnecting pores, pores diameter ranging from several tens to

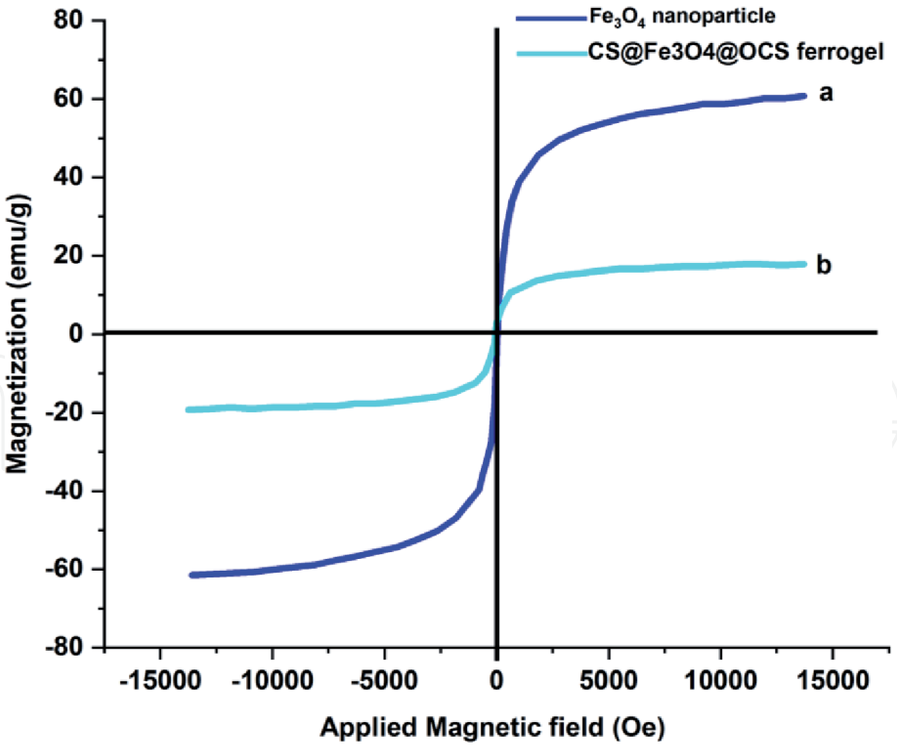


Figure 11.
The magnetic hysteresis loops for Fe_3O_4 NPs and CS@Fe_3O_4@OCS hydrogel measured by SQUID at room temperature.

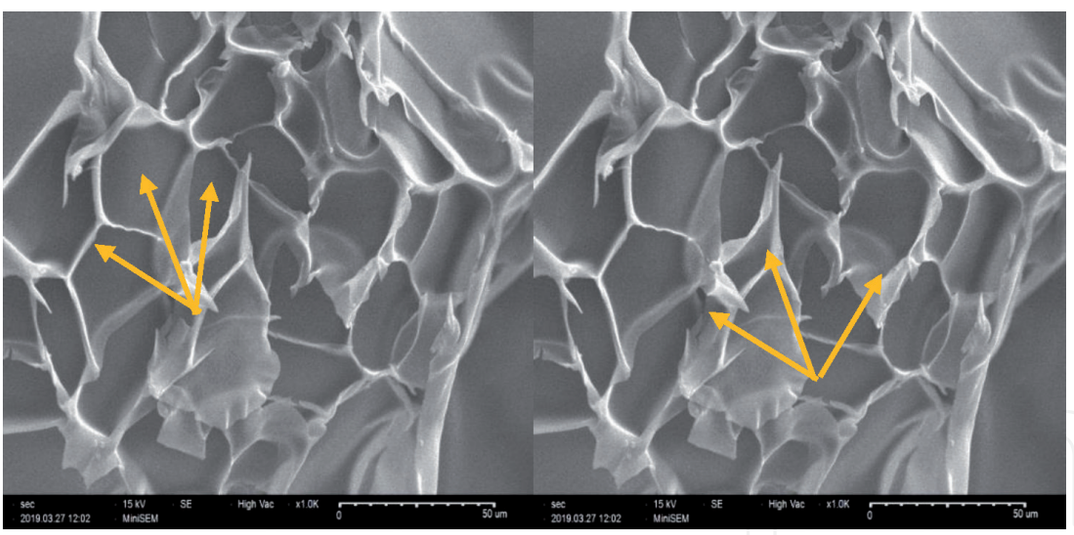


Figure 12.
Micrographs of chitosan cross-linked oxidized chitosan hydrogel at low and high magnification.

several thousands of micrometers [55]. Moreover, the more crosslinking between amino group and aldehyde group, the diameter of the pores are decreased and the compactness of pores increased. The micrographs of CS/OCS hydrogel it was clearly observed that the hydrogel had a three-dimensional porous structure, which was beneficial for drug delivery systems.

3.5 Thermogravimetric (TGA) analysis

To evaluate the thermal stability of the chitosan (CS) oxidized chitosan (OCS) and (CS/OCS) lyophilized hydrogel, TGA thermograms were obtained as shown in (**Figure 13**). The TGA of pure chitosan shows two-stage weight loss in the range 40

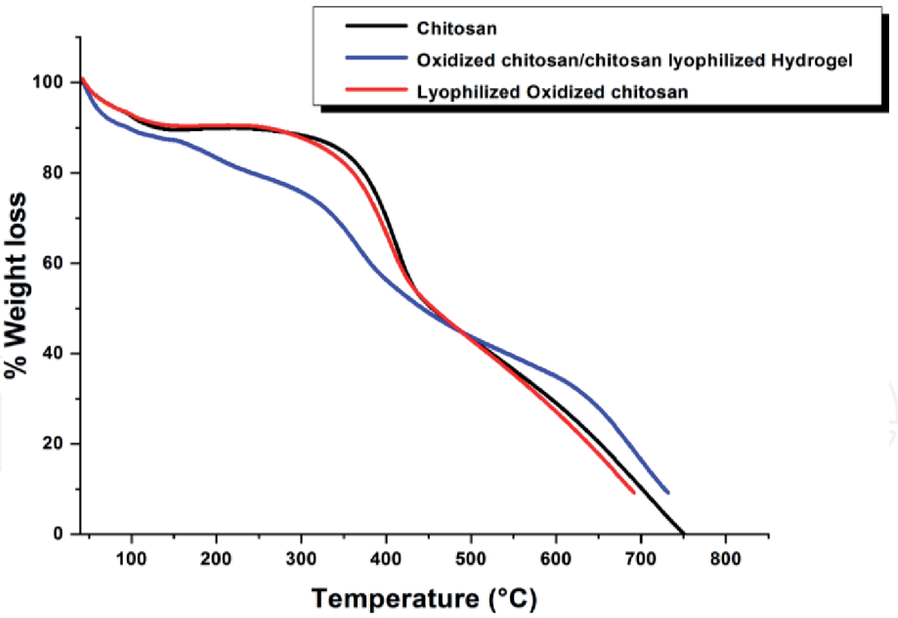


Figure 13.
TGA graphs of chitosan (CS), oxidized chitosan (OCS) and (CS/OCS) lyophilized hydrogel.

to 750°C (**Figure 13**), it is clear that chitosan started to degrade at 40–130°C with 8% weight is due to the loss of water molecules. Initial decomposition around 130°C for pure chitosan can be attributed to the strong water adsorptive nature of chitosan. The second stage of degradation occurred at 340°C and continued up to 460°C [67]. There was 38.43% weight loss occurring in the second stage due to degradation of pure chitosan biopolymer and the temperature at which maximum degradation observed was 274.74°C. At the end of 750°C, the total weight loss of sample was 100% [54, 67]. TGA of oxidized chitosan (OCS) showed two steps of degradation (**Figure 13**), the first stage ranges between 40 and 130°C and shows about 8.2% loss in weight corresponded to water release for the initial step. The second stage decomposition was observed from 300°C and continued up to 460°C, during this time there was 39% weight loss due to the degradation of chitosan. At the end of 700°C, the total weight loss of sample was 90% [10, 54]. For CS/OCS lyophilized hydrogel, the degradation starts at a lower temperature compared to chitosan and oxidized chitosan (**Figure 13**). For the CS/OCS hydrogel, shows two-stage weight loss in three stages. The first stages of degradation takes place from 40 to 160°C with a weight loss of 13% could be due to the loss of both the loosely bound water and tightly bound water [68]. The free water and hydrogen-bonded water are released at a temperature between 40 and 100°C. The hydrogel contains many hydrophilic groups that retain water more tightly in the hydrogel skeleton by polar interaction. As a result, it is harder to lose. Thus, this tightly bound water is released in the temperature region 100–156°C. The second stage of hydrogel degradation started between 160° C and 385° C with a 41% weight loss. The three-stages of degradation biopolymers, at the end of 700°C, the total weight loss of sample was 90%. This phase of the weight loss mainly could be caused by a series of thermal and oxidative decomposition in the process including dehydration of the sugar cycle, degradation, N-deacetylation of the molecular chain of the chitosan cracking unit and vaporization and removal of volatile products. It can be concluded the TGA curve shows at about 222°C. This is probably due to the formation of (-C=N-) and this proves that biopolymer-based Schiff base is thermally less stable.

The TGA curves of uncoated Fe_3O_4 and the lyophilized ferrogel (CS-Fe_3O_4-OCS) are shown in **Figure 14**. For uncoated Fe_3O_4 NPs (**Figure 14(a)**), the TGA curve showed that the weight loss over the temperature range 40–750°C was about 2.2%.

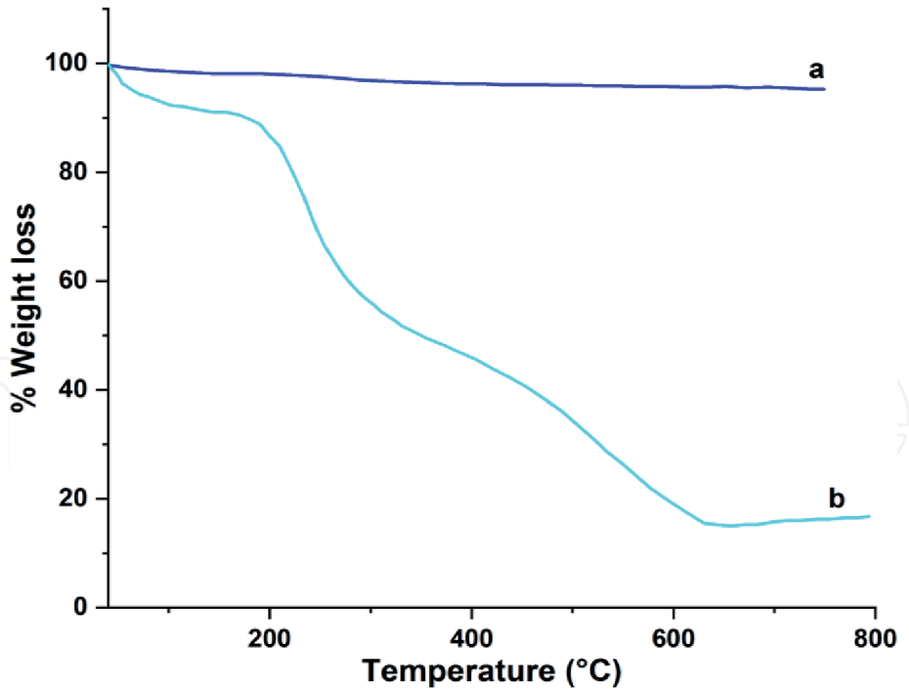


Figure 14.
TGA curves for a) uncoated Fe_3O_4 b) CS-Fe_3O_4-OCS lyophilized ferrogel.

Hence, this weight loss is related to removal of the physically adsorbed water and/or hydroxyl groups on the surface of Fe_3O_4 nanoparticles. For coated nanoparticles Fe_3O_4. Similarly, the weight curve of CS/Fe_3O_4/OCS (**Figure 14(b)**) showed a progressive decrease of 85%. This is due to the degradation of the polymer and hydrogen-bound water in the temperature range of 40–166°C, which forms the polysaccharide structure of OCS and CS. In addition, a uniform and steady decrease in weight loss at 166–630°C is CS/Fe_3O_4/OCS was observed. This may be partly attributed to the degradation and decomposition of organic skeletal structure, amino groups, and other functional groups. By comparing the curves of CS/Fe_3O_4/OCS and Fe_3O_4, it was observed that Fe_3O_4 particles are wrapped into CS and OCS can enhance the thermal stability of the whole system. A temperature of 630°C or higher, the remaining material was carbonized completely. The indicated that chitosan and oxidized chitosan coated Fe_3O_4 successfully and penetrated deeply into in the matrix CS/OCS.

3.6 Hydrogel swelling

To investigate the pH dependent swelling behavior of the CS/OCS hydrogels for drug delivery, PBS with (pH = 1.2; pH = 5.8 and pH = 7.4) at T = 37°C were used to simulate the physiological medium and were used for testing swelling of the hydrogels. The results of the equilibrium-swelling ratio are presented in (**Figure 15**). The CS/OCS hydrogels showed large differences in swelling behavior at different pH values. The pK_a value of the D-glucosamine residue in chitosan was approximately 6.2 to 7.0. Therefore, the amino groups in the chitosan were protonated and positively charged in acidic PBS (pH = 1.2 and pH = 5.8), and the electrostatic repulsion between positively charged -NH^{3+} groups would lead to swelling of the hydrogels. The % equilibrium swelling values were found to be higher at pH = 1.2, than at pH = 7.4. This can be explained by protonation of the unreacted NH_2 groups of chitosan at acidic pH, leading to dissociation of the hydrogen bonding involving the amino groups, and thus facilitating the entry of the solvent into the material. The swelling process of hydrogels involves the ionization [69]. Furthermore, the Schiff base bonds

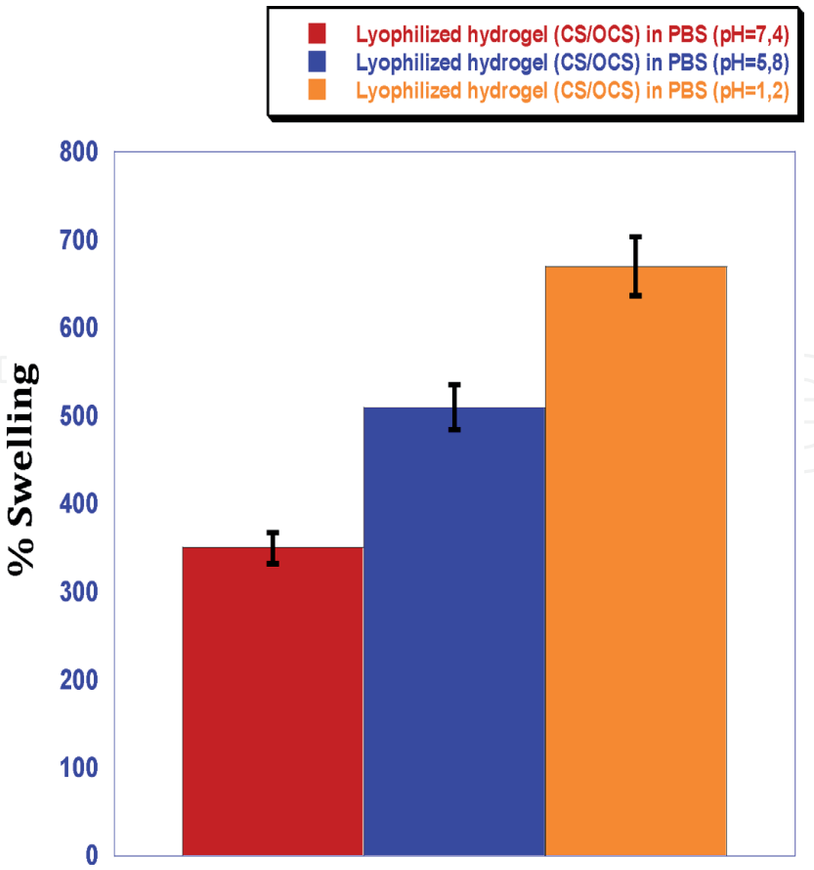


Figure 15.
% Swelling of CS/OCS hydrogel in buffer solutions of pH = 1,2, pH = 5,8 and pH = 7,4 at T = 37°C.

between -NH_2 and -CHO as a cross-linker became weak in PBS (pH = 7.4 at 37°C); the swelling ratio of CS/OCS was 350%, resulting in swelling of the hydrogel. Therefore, the CS/OCS hydrogel in PBS (pH = 1.2 at 37°C) exhibited the largest swelling ratio of 670%; the swelling ratio (pH = 5.8 at 37°C) was 509%. The decreased swelling ratio occurred due to increased crosslinking density in the hydrogels. Meanwhile, the equilibrium swelling ratios of the hydrogels in a pH = 7.4 solution dramatically decreased. This is because hydrogels exhibited pH-responsive swelling behavior, and the hydrogels showed a much higher swelling ratio in an acidic medium than that in a pH 7.4 medium.

3.7 In vitro release from the hydrogels

The model drugs (5-FU, caffeine and ascorbic acid) was encapsulated in the hydrogel matrix used for the release kinetics in PBS (pH = 7.4 at 37°C) are depicted in (**Figure 16**). The purpose here was to study whether the release of the drug trapped in the hydrogels, as well as by the simple diffusion. In a system, where drug is entrapped in a biodegradable matrix, the release rate depends on three parameters: the size of the drug molecule, the drug solubility (soluble-sparingly soluble-insoluble), the cross-linking density and the degradation rate. The ability of the chitosan-imine-oxidized chitosan hydrogels to act as matrix for controlled release was investigated in vitro by monitoring the release profile of the (5-FU, caffeine and ascorbic acid) three-model drug from system in phosphate buffer of physiological pH (7.4), at the human body temperature of 37°C (**Figure 16**). In order to study the release behavior of 5-FU, caffeine, ascorbic acid incorporated in the chitosan-based hydrogel cross-linked by oxidized chitosan, they were incubated in release media (phosphate buffer pH = 7.4 at 37°C) and evaluated by UV spectrophotometry.

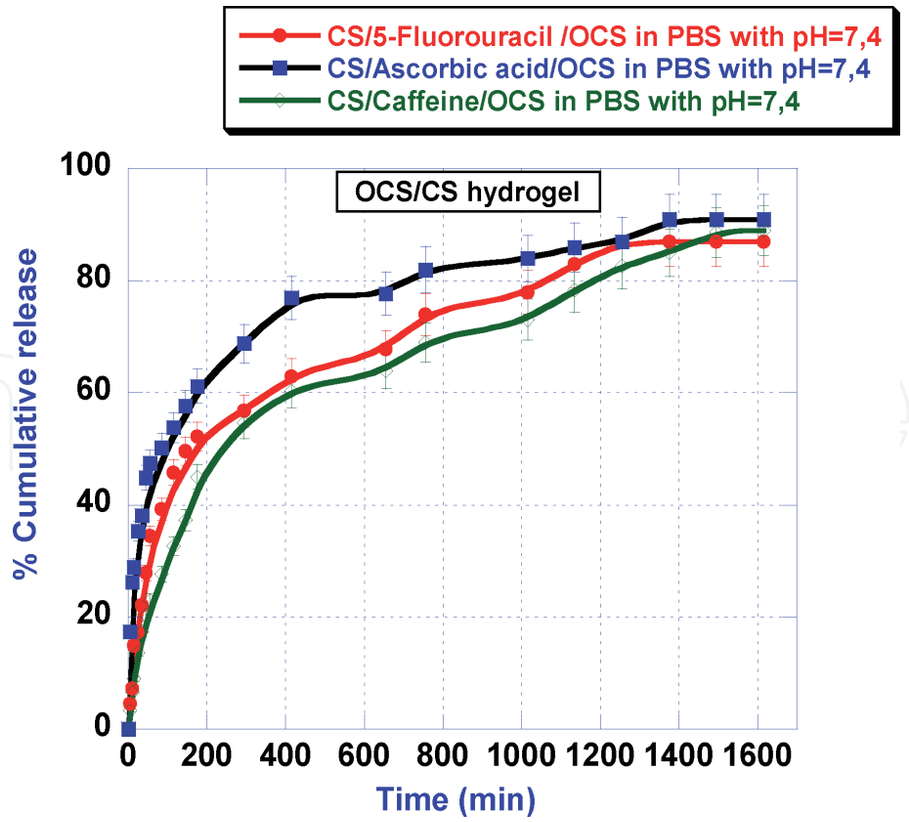


Figure 16.
In vitro release of 5-FU, caffeine and ascorbic acid embedded in hydrogels (pH = 7,4 at 37°C). Values reported are an average of n = 3 ± standard deviation.

(**Figure 16**) shows release profiles of 5-FU, caffeine and ascorbic acid up to 26 h of incubation period. As shown in (**Figure 16**), the chitosan hydrogels showed an initial burst release of 5-FU, caffeine and ascorbic acid over a period of 3 h for all incubation media, which was of the order of (5 -FU "52%", caffeine "43%" and ascorbic acid "60%"). This initial rapid release, characterized by a "burst effect», because certain quantities of 5-FU, caffeine and ascorbic acid were localized on the surface of the hydrogels by adsorption which could be released easily by diffusion. After 3h the release percentages of (5-FU "86%", caffeine "89%" and ascorbic acid "91%"), respectively [70]. The remaining part of the drug can be trapped in hydrogels because the amino functions of chitosan can enter into the Schiff reaction with the aldehyde groups of oxidized chitosan. Indeed, the hydrogel contained large pore size, which is beneficial for the diffusion of the drug, this initial bursting effect, a slower sustained and controlled release occurred throughout the incubation period and the amount of release. The release profiles confirmed that the (5-FU, caffeine and ascorbic acid) drugs were encapsulated in hydrogels.

As shown in **Figure 17**, magneto-hydrogel showed an initial burst release of (5-FU, caffeine and ascorbic acid) in a period of 5 h, which was in the range of (37%, 34%, and 42%). The initial burst phase is caused by drug adsorbed on the surface of the nanoparticles Fe_3O_4 embedded in hydrogel. The release kinetics at pH = 7.4 at 37°C within 45 h clearly indicated that Fe_3O_4 embedded in hydrogel influenced drugs release. At pH = 7.4 at 37°C, about (95%, 93% and 97%) amounts of 5-FU, caffeine and ascorbic acid were release after 45 h, respectively. Due to the slower swelling rate of nanotransporters in solution, the rate of drug release is also slower. It is well known that there are a large number of amino and hydroxyl groups on the surface of chitosan molecules, which provide functional groups and favorable characteristics for biological molecules. In PBS (pH = 7.4 at 37°C), amino

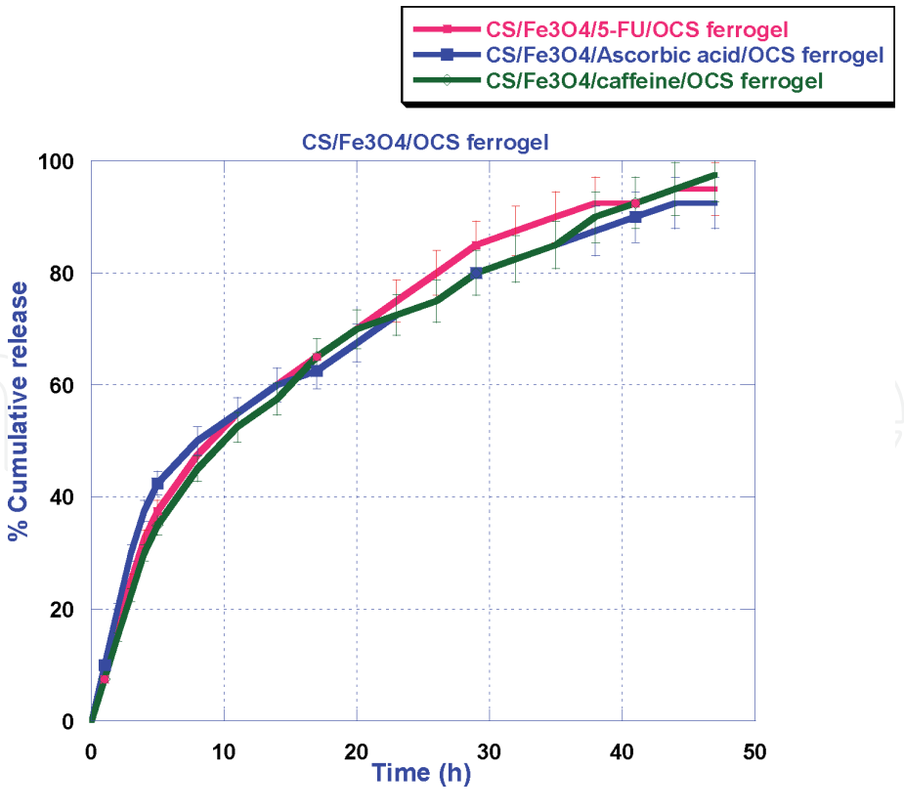


Figure 17.
Cumulative release profiles of 5-FU-gel, caffeine-gel, ascorbic acid-gel with external magnetic field. Values reported are an average of n = 3 ± standard deviation.

groups of chitosan mainly attach to the surface of the nanoparticles, so as to reduce the surface voids and render the pore blockage, lower penetration, and thus slow down the release rate of the drug [36]. However, due to the magnetic orientation role of MNPs, magnetic nano-drug carriers could be transported by applying an external magnetic field and maintain drug concentration for extended periods. Such rapid transport and slow release of the nanocarriers to the target site may be desirable for many biomedical applications, minimizing drug leakage to undesirable sites and reducing the risk of heart attack due to high dose in a short period of time. These results clearly illustrated that the chitosan hydrogel containing Fe_3O_4 resulted in a barrier system for the sustained release of 5-Fu, caffeine and ascorbic acid. We speculate that this barrier structure would block the drug loss in the early burst release, which is benefit to reduce the toxic side effects.

4. Conclusion

Many conclusions can be made from the present work, the ferrogels (FG) are cross-linked polymer networks containing magnetic nanoparticles: a) magnetic magnetite (Fe_3O_4) were synthesized successfully by chemical co-precipitation and has been confirmed using FT-IR, VSM analysis, TGA. The advantage of the co-precipitation method are low cost, rapidity, ease, reproducibility and high-yield synthesis. b) The hydrogel was formulated by cross-linking chitosan (CS) and oxidized chitosan (OCS) via the Schiff-base (-C=N-) reaction. Obviously, these results indicate that this exhibit non-toxic, biodegradable, good injectability, less expensive and respect the environment, quick gelation time, in vitro pH-dependent equilibrated swelling ratios, interconnected porosity. c) Magneto-responsive hydrogels are typically prepared by incorporating magnetic particles into hydrogels

and has been confirmed using (FT-IR), (TGA), (VSM) analysis at room temperature. d) The role of Fe_3O_4 embedded in hydrogel, which allows reducing the surface voids and rendering the pore blockage, lower penetration, and thus slowing down the release rate of the drug. e) A 5-Fluorouracil (5-FU), caffeine and ascorbic acid release tests were used to demonstrate the excellent in vitro drug release behavior of these hydrogels and ferrogels. However, all these results indicate that this type of biomaterial based on chitosan with oxidized chitosan in the presence of the three drugs with different solubility for the preparation of hydrogels effective for the controlled release of the drug. Compared to other hydrogels based on chitosan, the present study brings to the attention of researchers a novel strategy to design a non-toxic and biodegradable matrix for drug delivery systems, by the simple use of appropriate oxidized chitosan without incorporating any crosslinking agents. This design expands the variety of hydrogel matrices, guiding additional efforts in the development of the new ideas for pharmaceuticals applications. As a perspective and future challenges, we will test this type of ferrogels for cancer treatment by hyperthermia.

Author details

Damiri Fouad*, Yahya Bachra, Grouli Ayoub, Amine Ouaket, Ahmed Bennamara, Noureddine Knouzi and Mohammed Berrada
University Hassan II of Casablanca, Faculty of Sciences Ben M'Sick, Department of Chemistry, Laboratory of Biomolecules and Organic Synthesis (BIOSYNTHO), Casablanca, Morocco

*Address all correspondence to: fouad.damiri@outlook.fr

IntechOpen

© 2020 The Author(s). Licensee IntechOpen. This chapter is distributed under the terms of the Creative Commons Attribution License (http://creativecommons.org/licenses/by/3.0), which permits unrestricted use, distribution, and reproduction in any medium, provided the original work is properly cited. CC BY

References

[1] L. Boyle, P. & Bernard, World Cancer Report 2008, (IARC Press. Lyon). (2008) (IARC Press. Lyon).

[2] X.-J. Liang, C. Chen, Y. Zhao, P.C. Wang, Circumventing Tumor Resistance to Chemotherapy by Nanotechnology, in: 2010: pp. 467-488. https://doi.org/10.1007/978-1-60761-416-6_21.

[3] B. GAIHRE, M. KHIL, D. LEE, H. KIM, Gelatin-coated magnetic iron oxide nanoparticles as carrier system: Drug loading and in vitro drug release study, Int. J. Pharm. 365 (2009) 180-189. https://doi.org/10.1016/j.ijpharm.2008.08.020.

[4] J. Chomoucka, J. Drbohlavova, D. Huska, V. Adam, R. Kizek, J. Hubalek, Magnetic nanoparticles and targeted drug delivering, Pharmacol. Res. 62 (2010) 144-149. https://doi.org/10.1016/j.phrs.2010.01.014.

[5] R. Sensenig, Y. Sapir, C. MacDonald, S. Cohen, B. Polyak, Magnetic nanoparticle-based approaches to locally target therapy and enhance tissue regeneration in vivo, Nanomedicine. 7 (2012) 1425-1442. https://doi.org/10.2217/nnm.12.109.

[6] G.S. Dhillon, S. Kaur, S.K. Brar, M. Verma, Green synthesis approach: extraction of chitosan from fungus mycelia, Crit. Rev. Biotechnol. 33 (2013) 379-403. https://doi.org/10.3109/07388551.2012.717217.

[7] R.N. Tharanathan, F.S. Kittur, Chitin — The Undisputed Biomolecule of Great Potential, Crit. Rev. Food Sci. Nutr. 43 (2003) 61-87. https://doi.org/10.1080/10408690390826455.

[8] B.K. Park, M.-M. Kim, Applications of Chitin and Its Derivatives in Biological Medicine, Int. J. Mol. Sci. 11 (2010) 5152-5164. https://doi.org/10.3390/ijms11125152.

[9] V. Manigandan, R. Karthik, S. Ramachandran, S. Rajagopal, Chitosan Applications in Food Industry, in: Biopolym. Food Des., Elsevier, 2018: pp. 469-491. https://doi.org/10.1016/B978-0-12-811449-0.00015-3.

[10] A. Laaraibi, F. Moughaoui, F. Damiri, A. Ouakit, I. Charhouf, S. Hamdouch, A. Jaafari, A. Abourriche, N. Knouzi, A. Bennamara, M. Berrada, Chitosan-Clay Based (CS-NaBNT) Biodegradable Nanocomposite Films for Potential Utility in Food and Environment, in: Chitin-Chitosan - Myriad Funct. Sci. Technol., InTech, 2018. https://doi.org/10.5772/intechopen.76498.

[11] I. Aranaz, N. Acosta, C. Civera, B. Elorza, J. Mingo, C. Castro, M. Gandía, A. Heras Caballero, Cosmetics and Cosmeceutical Applications of Chitin, Chitosan and Their Derivatives, Polymers (Basel). 10 (2018) 213. https://doi.org/10.3390/polym10020213.

[12] J. Roy, F. Salaün, S. Giraud, A. Ferri, J. Guan, Chitosan-Based Sustainable Textile Technology: Process, Mechanism, Innovation, and Safety, in: Biol. Act. Appl. Mar. Polysaccharides, InTech, 2017. https://doi.org/10.5772/65259.

[13] R. Sharp, A Review of the Applications of Chitin and Its Derivatives in Agriculture to Modify Plant-Microbial Interactions and Improve Crop Yields, Agronomy. 3 (2013) 757-793. https://doi.org/10.3390/agronomy3040757.

[14] M.C. Gortari, R.A. Hours, Biotechnological processes for chitin recovery out of crustacean waste: A mini-review, Electron. J. Biotechnol. 16 (2013). https://doi.org/10.2225/vol16-issue3-fulltext-10.

[15] G. Tiwari, R. Tiwari, S. Bannerjee, L. Bhati, S. Pandey, P. Pandey, B.

Sriwastawa, Drug delivery systems: An updated review, Int. J. Pharm. Investig. 2 (2012) 2. https://doi.org/10.4103/2230-973X.96920.

[16] N. Kamaly, B. Yameen, J. Wu, O.C. Farokhzad, Degradable Controlled-Release Polymers and Polymeric Nanoparticles: Mechanisms of Controlling Drug Release, Chem. Rev. 116 (2016) 2602-2663. https://doi.org/10.1021/acs.chemrev.5b00346.

[17] P. Baldrick, The safety of chitosan as a pharmaceutical excipient, Regul. Toxicol. Pharmacol. 56 (2010) 290-299. https://doi.org/10.1016/j.yrtph.2009.09.015.

[18] E. Ruel-Gariépy, M. Shive, A. Bichara, M. Berrada, D. Le Garrec, A. Chenite, J.-C. Leroux, A thermosensitive chitosan-based hydrogel for the local delivery of paclitaxel, Eur. J. Pharm. Biopharm. 57 (2004) 53-63. https://doi.org/10.1016/S0939-6411(03)00095-X.

[19] M.E. Parente, A. Ochoa Andrade, G. Ares, F. Russo, Á. Jiménez-Kairuz, Bioadhesive hydrogels for cosmetic applications, Int. J. Cosmet. Sci. 37 (2015) 511-518. https://doi.org/10.1111/ics.12227.

[20] B. Cheng, B. Pei, Z. Wang, Q. Hu, Advances in chitosan-based superabsorbent hydrogels, RSC Adv. 7 (2017) 42036-42046. https://doi.org/10.1039/C7RA07104C.

[21] D. Huber, G. Tegl, M. Baumann, E. Sommer, E.G. Gorji, N. Borth, G. Schleining, G.S. Nyanhongo, G.M. Guebitz, Chitosan hydrogel formation using laccase activated phenolics as cross-linkers, Carbohydr. Polym. 157 (2017) 814-822. https://doi.org/10.1016/j.carbpol.2016.10.012.

[22] M. Periayah, A. Halim, A.M. Saad, Chitosan: A promising marine polysaccharide for biomedical research, Pharmacogn. Rev. 10 (2016) 39. https://doi.org/10.4103/0973-7847.176545.

[23] M.A. Elgadir, M.S. Uddin, S. Ferdosh, A. Adam, A.J.K. Chowdhury, M.Z.I. Sarker, Impact of chitosan composites and chitosan nanoparticle composites on various drug delivery systems: A review, J. Food Drug Anal. 23 (2015) 619-629. https://doi.org/10.1016/j.jfda.2014.10.008.

[24] T. Kean, M. Thanou, Biodegradation, biodistribution and toxicity of chitosan, Adv. Drug Deliv. Rev. 62 (2010) 3-11. https://doi.org/10.1016/j.addr.2009.09.004.

[25] J.-Q. Gao, Hu, Wang, Han, Toxicity evaluation of biodegradable chitosan nanoparticles using a zebrafish embryo model, Int. J. Nanomedicine. (2011) 3351. https://doi.org/10.2147/IJN.S25853.

[26] A.S. Kritchenkov, S. Andranovitš, Y.A. Skorik, Chitosan and its derivatives: vectors in gene therapy, Russ. Chem. Rev. 86 (2017) 231-239. https://doi.org/10.1070/RCR4636.

[27] H. Sashiwa, Y. Shigemasa, Chemical modification of chitin and chitosan 2: preparation and water soluble property of N-acylated or N-alkylated partially deacetylated chitins, Carbohydr. Polym. 39 (1999) 127-138. https://doi.org/10.1016/S0144-8617(98)00167-2.

[28] M.S. Benhabiles, R. Salah, H. Lounici, N. Drouiche, M.F.A. Goosen, N. Mameri, Antibacterial activity of chitin, chitosan and its oligomers prepared from shrimp shell waste, Food Hydrocoll. 29 (2012) 48-56. https://doi.org/10.1016/j.foodhyd.2012.02.013.

[29] J. Cao, L. Xiao, X. Shi, Injectable drug-loaded polysaccharide hybrid hydrogels for hemostasis, RSC Adv. 9 (2019) 36858-36866. https://doi.org/10.1039/C9RA07116D.

[30] M. Dash, F. Chiellini, R.M. Ottenbrite, E. Chiellini, Chitosan—A versatile semi-synthetic polymer in biomedical applications, Prog. Polym. Sci. 36 (2011) 981-1014. https://doi.org/10.1016/j.progpolymsci.2011.02.001.

[31] M. Huang, E. Khor, L.-Y. Lim, Uptake and Cytotoxicity of Chitosan Molecules and Nanoparticles: Effects of Molecular Weight and Degree of Deacetylation, Pharm. Res. 21 (2004) 344-353. https://doi.org/10.1023/B:PHAM.0000016249.52831.a5.

[32] R. Spanneberg, F. Osswald, I. Kolesov, W. Anton, H.-J. Radusch, M.A. Glomb, Model Studies on Chemical and Textural Modifications in Gelatin Films by Reaction with Glyoxal and Glycolaldehyde, J. Agric. Food Chem. 58 (2010) 3580-3585. https://doi.org/10.1021/jf9039827.

[33] M.P. Shaffer, D. V. Belsito, Allergic contact dermatitis from glutaraldehyde in health-care workers, Contact Dermatitis. 43 (2000) 150-156. https://doi.org/10.1034/j.1600-0536.2000.043003150.x.

[34] F. Damiri, Y. Bachra, C. Bounacir, A. Laaraibi, M. Berrada, Synthesis and Characterization of Lyophilized Chitosan-Based Hydrogels Cross-Linked with Benzaldehyde for Controlled Drug Release, J. Chem. 2020 (2020) 1-10. https://doi.org/10.1155/2020/8747639.

[35] H.W. Sung, R.N. Huang, L.L. Huang, C.C. Tsai, In vitro evaluation of cytotoxicity of a naturally occurring cross-linking reagent for biological tissue fixation., J. Biomater. Sci. Polym. Ed. 10 (1999) 63-78. https://doi.org/10.1163/156856299x00289.

[36] X. Chen, M. Fan, H. Tan, B. Ren, G. Yuan, Y. Jia, J. Li, D. Xiong, X. Xing, X. Niu, X. Hu, Magnetic and self-healing chitosan-alginate hydrogel encapsulated gelatin microspheres via covalent cross-linking for drug delivery, Mater. Sci. Eng. C. 101 (2019) 619-629. https://doi.org/10.1016/j.msec.2019.04.012.

[37] B.Y. Shin, B.G. Cha, J.H. Jeong, J. Kim, Injectable Macroporous Ferrogel Microbeads with a High Structural Stability for Magnetically Actuated Drug Delivery, ACS Appl. Mater. Interfaces. 9 (2017) 31372-31380. https://doi.org/10.1021/acsami.7b06444.

[38] R. Lamouri, L. Fkhar, E. Salmani, O. Mounkachi, M. Hamedoun, M. Ait Ali, A. Benyoussef, H. Ez-Zahraouy, A combined experimental and theoretical study of the magnetic properties of bulk CoFe2O4, Appl. Phys. A. 126 (2020) 325. https://doi.org/10.1007/s00339-020-03510-9.

[39] R. Lamouri, O. Mounkachi, E. Salmani, M. Hamedoun, A. Benyoussef, H. Ez-Zahraouy, Size effect on the magnetic properties of CoFe2O4 nanoparticles: A Monte Carlo study, Ceram. Int. 46 (2020) 8092-8096. https://doi.org/10.1016/j.ceramint.2019.12.035.

[40] R. Muzzalupo, L. Tavano, C.O. Rossi, N. Picci, G.A. Ranieri, Novel pH sensitive ferrogels as new approach in cancer treatment: Effect of the magnetic field on swelling and drug delivery, Colloids Surfaces B Biointerfaces. 134 (2015) 273-278. https://doi.org/10.1016/j.colsurfb.2015.06.065.

[41] T. Guo, X. Bian, C. Yang, A new method to prepare water based Fe3O4 ferrofluid with high stabilization, Phys. A Stat. Mech. Its Appl. 438 (2015) 560-567. https://doi.org/10.1016/j.physa.2015.06.035.

[42] Z.-X. Li, D. Luo, M.-M. Li, X.-F. Xing, Z.-Z. Ma, H. Xu, Recyclable Fe3O4 Nanoparticles Catalysts for Aza-Michael Addition of Acryl Amides by

Magnetic Field, Catalysts. 7 (2017) 219. https://doi.org/10.3390/catal7070219.

[43] Z.R. Stephen, F.M. Kievit, M. Zhang, Magnetite nanoparticles for medical MR imaging, Mater. Today. 14 (2011) 330-338. https://doi.org/10.1016/S1369-7021(11)70163-8.

[44] J. Kim, V.T. Tran, S. Oh, C.-S. Kim, J.C. Hong, S. Kim, Y.-S. Joo, S. Mun, M.-H. Kim, J.-W. Jung, J. Lee, Y.S. Kang, J.-W. Koo, J. Lee, Scalable Solvothermal Synthesis of Superparamagnetic Fe 3 O 4 Nanoclusters for Bioseparation and Theragnostic Probes, ACS Appl. Mater. Interfaces. 10 (2018) 41935-41946. https://doi.org/10.1021/acsami.8b14156.

[45] J. Jose, R. Kumar, S. Harilal, G.E. Mathew, D.G.T. Parambi, A. Prabhu, M.S. Uddin, L. Aleya, H. Kim, B. Mathew, Magnetic nanoparticles for hyperthermia in cancer treatment: an emerging tool, Environ. Sci. Pollut. Res. 27 (2020) 19214-19225. https://doi.org/10.1007/s11356-019-07231-2.

[46] A. Radoń, A. Drygała, Ł. Hawełek, D. Łukowiec, Structure and optical properties of Fe 3 O 4 nanoparticles synthesized by co-precipitation method with different organic modifiers, Mater. Charact. 131 (2017) 148-156. https://doi.org/10.1016/j.matchar.2017.06.034.

[47] O.M. Lemine, K. Omri, B. Zhang, L. El Mir, M. Sajieddine, A. Alyamani, M. Bououdina, Sol–gel synthesis of 8nm magnetite (Fe3O4) nanoparticles and their magnetic properties, Superlattices Microstruct. 52 (2012) 793-799. https://doi.org/10.1016/j.spmi.2012.07.009.

[48] W. Zhang, F. Shen, R. Hong, Solvothermal synthesis of magnetic Fe3O4 microparticles via self-assembly of Fe3O4 nanoparticles, Particuology. 9 (2011) 179-186. https://doi.org/10.1016/j.partic.2010.07.025.

[49] D. Stadler, D.N. Mueller, T. Brede, T. Duchoň, T. Fischer, A. Sarkar, M. Giesen, C.M. Schneider, C.A. Volkert, S. Mathur, Magnetic Field-Assisted Chemical Vapor Deposition of Iron Oxide Thin Films: Influence of Field–Matter Interactions on Phase Composition and Morphology, J. Phys. Chem. Lett. 10 (2019) 6253-6259. https://doi.org/10.1021/acs.jpclett.9b02381.

[50] R. Weissleder, A. Bogdanov, E.A. Neuwelt, M. Papisov, Long-circulating iron oxides for MR imaging, Adv. Drug Deliv. Rev. 16 (1995) 321-334. https://doi.org/10.1016/0169-409X(95)00033-4.

[51] S. Mitragotri, J. Lahann, Physical approaches to biomaterial design, Nat. Mater. 8 (2009) 15-23. https://doi.org/10.1038/nmat2344.

[52] Z. Lu, M.D. Prouty, Z. Guo, V.O. Golub, C.S.S.R. Kumar, Y.M. Lvov, Magnetic Switch of Permeability for Polyelectrolyte Microcapsules Embedded with Co@Au Nanoparticles, Langmuir. 21 (2005) 2042-2050. https://doi.org/10.1021/la047629q.

[53] P.J. Reséndiz-Hernández, O.S. Rodríguez-Fernández, L.A. García-Cerda, Synthesis of poly(vinyl alcohol)–magnetite ferrogel obtained by freezing–thawing technique, J. Magn. Magn. Mater. 320 (2008) e373–e376. https://doi.org/10.1016/j.jmmm.2008.02.073.

[54] B.M. Charhouf I, Bennamara A, Abourriche A, Chenite A, Zhu J, Characterization of a Dialdehyde Chitosan Generated by Periodate Oxidation, Int. J. Sci. Basic Appl. Res. 16(2) (2014) 336-348.

[55] H. Tan, C.R. Chu, K.A. Payne, K.G. Marra, Injectable in situ forming biodegradable chitosan–hyaluronic acid based hydrogels for cartilage tissue engineering, Biomaterials. 30 (2009) 2499-2506. https://doi.org/10.1016/j.biomaterials.2008.12.080.

[56] L. Liu, X. Tang, Y. Wang, S. Guo, Smart gelation of chitosan solution in the presence of NaHCO3 for injectable drug delivery system, Int. J. Pharm. 414 (2011) 6-15. https://doi.org/10.1016/j.ijpharm.2011.04.052.

[57] R.W. Korsmeyer, R. Gurny, E. Doelker, P. Buri, N.A. Peppas, Mechanisms of solute release from porous hydrophilic polymers, Int. J. Pharm. 15 (1983) 25-35. https://doi.org/10.1016/0378-5173(83)90064-9.

[58] C. Müller, D. Rahmat, F. Sarti, K. Leithner, A. Bernkop-Schnürch, Immobilization of 2-mercaptoethylamine on oxidized chitosan: A substantially mucoadhesive and permeation enhancing polymer, J. Mater. Chem. 22 (2012) 3899-3908. https://doi.org/10.1039/c2jm15164b.

[59] M. Fernandes Queiroz, K. Melo, D. Sabry, G. Sassaki, H. Rocha, Does the Use of Chitosan Contribute to Oxalate Kidney Stone Formation?, Mar. Drugs. 13 (2014) 141-158. https://doi.org/10.3390/md13010141.

[60] M. KASAAI, A review of several reported procedures to determine the degree of N-acetylation for chitin and chitosan using infrared spectroscopy, Carbohydr. Polym. 71 (2008) 497-508. https://doi.org/10.1016/j.carbpol.2007.07.009.

[61] Y. Jia, Y. Hu, Y. Zhu, L. Che, Q. Shen, J. Zhang, X. Li, Oligoamines conjugated chitosan derivatives: Synthesis, characterization, in vitro and in vivo biocompatibility evaluations, Carbohydr. Polym. 83 (2011) 1153-1161. https://doi.org/10.1016/j.carbpol.2010.09.046.

[62] M. Mehedi Hasan, M. Nuruzzaman Khan, P. Haque, M.M. Rahman, Novel alginate-di-aldehyde cross-linked gelatin/nano-hydroxyapatite bioscaffolds for soft tissue regeneration, Int. J. Biol. Macromol. 117 (2018) 1110-1117. https://doi.org/10.1016/j.ijbiomac.2018.06.020.

[63] Y. Wei, B. Han, X. Hu, Y. Lin, X. Wang, X. Deng, Synthesis of Fe3O4 Nanoparticles and their Magnetic Properties, Procedia Eng. 27 (2012) 632-637. https://doi.org/10.1016/j.proeng.2011.12.498.

[64] S. Lü, M. Liu, B. Ni, An injectable oxidized carboxymethylcellulose/N-succinyl-chitosan hydrogel system for protein delivery, Chem. Eng. J. 160 (2010) 779-787. https://doi.org/10.1016/j.cej.2010.03.072.

[65] Z. Zarnegar, J. Safari, Fe 3 O 4 @ chitosan nanoparticles: a valuable heterogeneous nanocatalyst for the synthesis of 2,4,5-trisubstituted imidazoles, RSC Adv. 4 (2014) 20932-20939. https://doi.org/10.1039/C4RA03176H.

[66] J. Wu, W. Jiang, R. Tian, Y. Shen, W. Jiang, Facile synthesis of magnetic-/pH-responsive hydrogel beads based on Fe 3 O 4 nanoparticles and chitosan hydrogel as MTX carriers for controlled drug release, J. Biomater. Sci. Polym. Ed. 27 (2016) 1553-1568. https://doi.org/10.1080/09205063.2016.1218212.

[67] H. Ghasemzadeh, M. Sheikhahmadi, F. Nasrollah, Full polysaccharide crosslinked-chitosan and silver nano composites, for use as an antibacterial membrane, Chinese J. Polym. Sci. 34 (2016) 949-964. https://doi.org/10.1007/s10118-016-1807-3.

[68] E.F.S. Vieira, A.R. Cestari, C. Airoldi, W. Loh, Polysaccharide-Based Hydrogels: Preparation, Characterization, and Drug Interaction Behaviour, Biomacromolecules. 9 (2008) 1195-1199. https://doi.org/10.1021/bm7011983.

[69] S.J. Kim, S.J. Park, S.I. Kim, Swelling behavior of interpenetrating polymer network hydrogels composed

of poly(vinyl alcohol) and chitosan, React. Funct. Polym. 55 (2003) 53-59. https://doi.org/10.1016/S1381-5148(02)00214-6.

[70] Y. Liang, X. Zhao, P.X. Ma, B. Guo, Y. Du, X. Han, pH-responsive injectable hydrogels with mucosal adhesiveness based on chitosan-grafted-dihydrocaffeic acid and oxidized pullulan for localized drug delivery, J. Colloid Interface Sci. 536 (2019) 224-234. https://doi.org/10.1016/j.jcis.2018.10.056.

IntechOpen